nature photonics

LETTERS

PUBLISHED ONLINE: 10 JANUARY 2010 | DOI: 10.1038/NPHOTON.2009.262

Highly power-efficient quantum cascade lasers

Peter Q. Liu[1]*, Anthony J. Hoffman[1], Matthew D. Escarra[1], Kale J. Franz[1], Jacob B. Khurgin[2], Yamac Dikmelik[2], Xiaojun Wang[3], Jen-Yu Fan[3] and Claire F. Gmachl[1]

Quantum cascade lasers[1] are promising mid-infrared semiconductor light sources for molecular detection in applications such as environmental sensing or medical diagnostics. For such applications, researchers have been striving to improve device performance[2]. Recently, improvements in wall plug efficiency have been pursued with a view to realizing compact, portable, power-efficient and high-power quantum cascade laser systems[3,4]. However, advances have largely been incremental, and the basic quantum design has remained unchanged for many years, with the wall plug efficiency yet to reach above 35%. A crucial factor in quantum cascade laser performance is the efficient transport of electrons into the laser active regions. We recently theoretically described this transport process as limited by the interface-roughness-induced detuning of resonant tunnelling[5]. Here, we report that an 'ultrastrong coupling' design strategy overcomes this limiting factor and leads to the experimental realization of quantum cascade lasers with 40–50% wall plug efficiency when operated in pulsed mode at temperatures of 160 K or lower.

Quantum cascade lasers (QCLs) are based on intersubband transitions in semiconductor quantum wells. Photons are generated when electrons transported into the active regions from the preceding injector regions undergo radiative transitions between the upper and lower laser levels and are subsequently extracted into the next downstream injector regions. The electron transport from an injector region into the next active region occurs by means of resonant tunnelling between the injector ground level and the upper laser level. The tunnelling rate, as well as many other performance-related parameters, can be engineered through quantum design, for example, through the design of the coupling strength, which is defined as half of the energy splitting between the injector ground level and the upper laser level when they are in full resonance. Theoretical analyses show that a fast tunnelling rate is a critical factor to achieving high laser wall plug efficiency (WPE)[6,7]. On the one hand, the faster the tunnelling rate, the higher the maximum operating current density that can be supported, and therefore the higher the current efficiency (that is, how far above threshold the laser is operated), which is an important factor of WPE. On the other hand, the internal efficiency and the gain also benefit from a faster tunnelling rate, because it reduces the electron population in the injector region, and thus minimizes the leakage current from the injector ground level to the lower laser level or the continuum energy levels and increases population inversion.

With practical growth techniques, interfaces between adjacent semiconductor layers are not perfectly smooth, but in fact are rather rough on the scale of atomic-layer steps of a few ångstroms[8], which is significant when compared to the typical semiconductor layer thicknesses of ~10–50 Å in QCLs. Furthermore, in the InGaAs/AlInAs/InP material system, different interfaces have generally unrelated roughness, because the width fluctuations of adjacent barriers and wells are unrelated. As a result, such interface roughness introduces significant detuning to the energy levels in resonance, which plays a crucial role in reducing the tunnelling rate between the injector and active regions and thus the laser WPE. This effect has been neglected until recently, so conventional designs have failed to incorporate an adequate mechanism with which to reduce its negative influence. We recently re-evaluated this effect and modelled its importance for laser gain[5]. Our theoretical calculations show that the interface-roughness-induced detuning to the resonant tunnelling has, in fact, a much greater effect than the broadening of the radiative transition that had previously been used as the limiting factor for electron transport and gain. With the coupling strength in conventional designs, the achieved gain is lower by a factor of 2 to 3 than the maximum achievable value, and the transport is also slowed by a factor of 2 to 3. One way to improve gain and transport is to significantly increase the coupling strength between the injector ground level and the upper laser level. Here, we report on the first experimental implementation of such a design strategy and the demonstration of QCLs with greatly improved

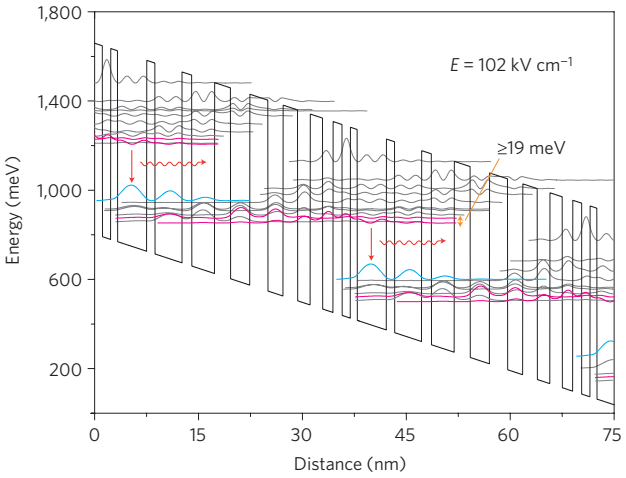

Figure 1 | A portion of the conduction band diagram of the ultra-strong coupling QCL design at an applied electric field of 102 kV cm^{-1}. The conduction band energy potential is plotted as black lines. Starting from the widest quantum well, the layer sequence of one period of the active and injector regions in the electron downstream direction (with individual thickness, in nanometres) is 4.2/**1.2**/3.9/**1.4**/3.3/**2.3**/2.8/**2.6**/2.2/**2.1**/1.8/**1.8**/1.5/**1.3**/1.2/**1.0**, where the InAlAs barriers are in bold and the InGaAs wells are in normal text. The underlined layers are doped with a doping density of 2.3×10^{17} cm^{-3}.The pairs of states in magenta are the coupled injector ground levels and upper laser levels, which have a ~19 meV energy splitting indicated by the orange arrow. The states in blue are the lower laser levels. Other states are in grey. The red arrows indicate the radiative transitions.

[1]Department of Electrical Engineering, Princeton University, Princeton, New Jersey 08544, USA, [2]Department of Electrical and Computer Engineering, Johns Hopkins University, Baltimore, Maryland 21218, USA, [3]AdTech Optics Inc., City of Industry, California 91748, USA. *e-mail: qiangliu@princeton.edu

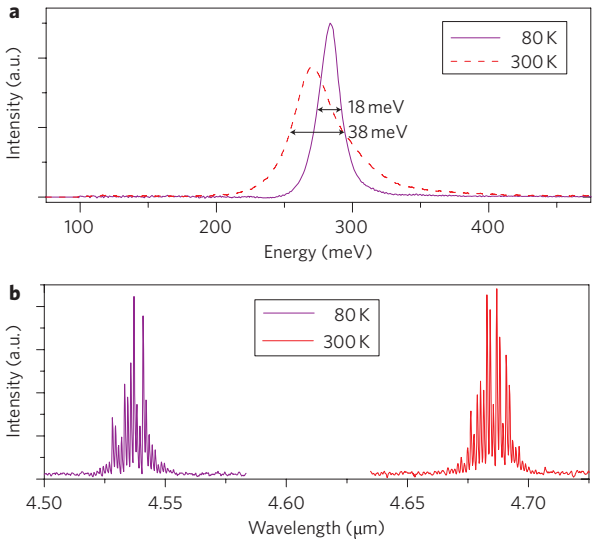

Figure 2 | Electroluminescence spectra and laser spectra. **a**, Electroluminescence spectra of the QC structure at 80 and 300 K with extracted full-width at half-maximum values. **b**, Laser spectra at 80 and 300 K.

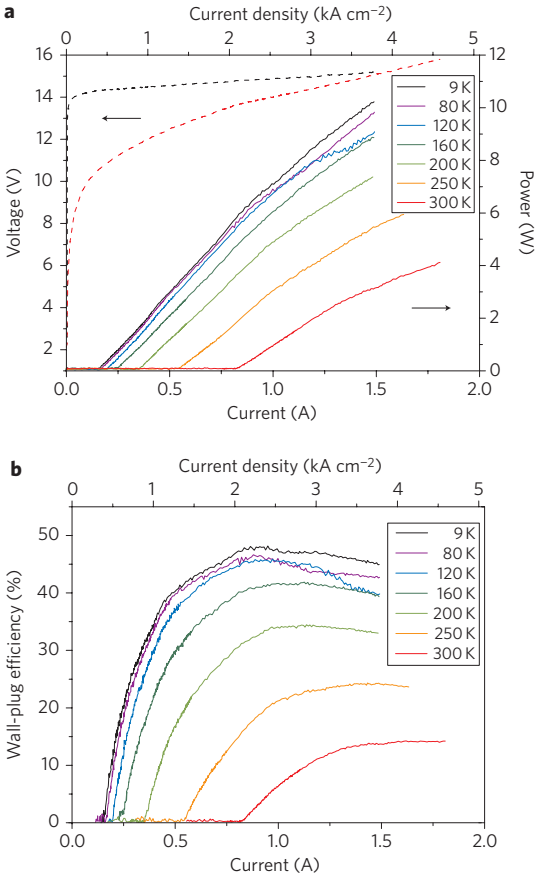

Figure 3 | Pulsed light–current–voltage measurements and extracted WPE. **a**, Pulsed light–current–voltage measurements for an as-cleaved 13.6-μm-wide, 2.9-mm-long QCL at various heat sink temperatures as indicated. The measured single-facet optical power is doubled for two facets (a process we have tested to be valid for as-cleaved Fabry–Perot QCLs) and corrected for an optical collection efficiency of 74% (calculated from far-field measurement of the laser, Supplementary Fig. S2). **b**, WPE versus current is extracted from the experimental results in **a** (not corrected for wiring resistance).

WPE at low temperatures. Our resulting new QCL design, shown in Fig. 1, uses a calculated optimal coupling strength of ∼10 meV, which is much stronger compared to those in conventional designs (∼2–4 meV). This is achieved by adopting a much thinner injection barrier (∼10 Å versus ∼30–40 Å in conventional designs) between the injector and active regions. This ultrastrong coupling effectively overcomes the interface-roughness-induced detuning of resonant tunnelling and therefore improves the latter. Furthermore, the tunnelling rate becomes less susceptible to changes in external bias. First, the stronger coupling leads to stronger anti-crossing and a reduced Stark shift (that is, the detuning due to the change in the electric field) between the injector ground and upper laser level, which consequently makes the alignment of the two energy levels more stable when subjected to a change in the external bias. Second, the tunnelling rate between the two coupled wavefunctions also becomes less susceptible to detuning from the full resonance (see Supplementary Information for details). Another concurrent advantage of this ultrastrong coupling design is that the upper laser level spreads more into the injector region because of the thin injection barrier, so that the radiative transition is more 'diagonal' rather than 'vertical'[2], which increases the upper laser level lifetime and eventually improves the slope efficiency and decreases the threshold current density. The active region design is based on three quantum wells, and two resonant longitudinal optical (LO) phonon scattering is adopted to depopulate the lower laser level[9]. This relatively low voltage defect also benefits the WPE at low temperatures. Overall, this work reported here focuses on improving the laser performance at low temperatures, as the fundamental physical properties of the lasers are usually better manifested at low temperatures.

The QCL structure was grown by metal organic chemical vapour deposition (MOCVD) on an InP substrate using strain-balanced $In_{0.66}Ga_{0.34}As/Al_{0.69}In_{0.31}As$ materials and consisted of a low-loss InP-based waveguide cladding on top of 43 repeats of the injector/active regions sequence. Each injector region had a sheet doping density of $1 \times 10^{11}cm^{-2}$. Ridge waveguide lasers were fabricated with ridge widths varying from 13.5–21.5 μm using conventional III–V semiconductor processing techniques. The ridges were wet-etched to a depth of ∼8 μm, an ∼0.3 μm SiO_x insulation layer was deposited with plasma-enhanced chemical vapour deposition (PECVD), thin 30 nm/300 nm titanium–gold top metal contacts were deposited through electron-beam evaporation, the substrate then thinned down to ∼200 μm and 20 nm/200 nm germanium–gold bottom metal contact deposited. Circular mesa samples with a diameter of ∼190 μm (for electroluminescence and electron transport measurements) were fabricated from the same wafer using similar techniques, except that no SiO_x insulation layer was required. Lasers with cavity lengths varying from 0.5 to 4.0 mm and as-cleaved facets were mounted epitaxial side up to copper heat sinks. Lasers with buried-heterostructure waveguides and a fixed cavity length of 1.9 mm were also fabricated, coated for high reflectivity on their back-facets, and mounted epitaxial side up.

Figure 2a shows the electroluminescence spectra of a mesa sample at 80 and 300 K. Contrary to expectations, the ultrastrong coupling in this design shows no obvious, if any, negative impact on the gain spectrum width. The radiative transition broadening is similar to that of the best comparable conventional designs. Characterization of the electron transport properties (current–voltage characteristics) on the non-lasing mesa samples show both higher maximum operating current densities and lower differential resistance for our ultrastrong coupling design across a large temperature range compared to an exemplary high-performance conventional design of similar wavelength and sheet doping density

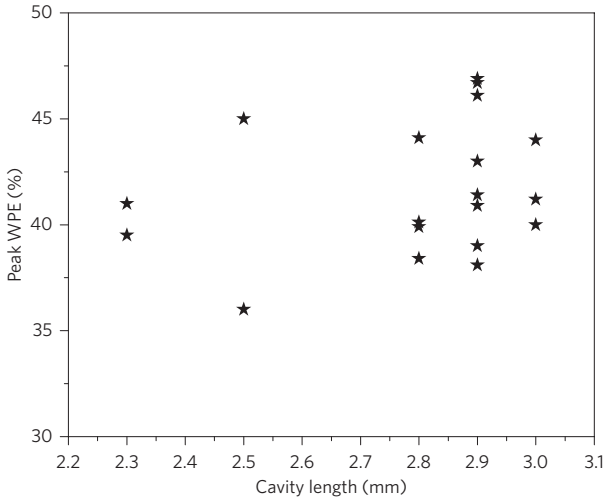

Figure 4 | Scatter plot of pulsed peak WPE at 80 K for all tested lasers with cavity lengths ranging from 2.3 to 3.0 mm. The majority of the tested devices in this cavity length range have a peak WPE greater than 40% at 80 K, and several have a peak WPE greater than 45% (this plot is not corrected for wiring resistance).

(Supplementary Fig. S1). Representative laser spectra are shown in Fig. 2b; the lasing wavelength is ~4.5 μm at cryogenic temperatures and ~4.7 μm at room temperature.

The laser characterization results show significant improvements in slope efficiency, peak power and WPE across a broad range of temperatures compared to those of the best reported QCLs at similar wavelengths and operating conditions[10]. For pulsed-mode operation (5 kHz repetition rate, 100 ns pulse width), one of the best performing lasers (a 13.6-μm-wide and 2.9-mm-long ridge) has a slope efficiency of ~8 W A^{-1}, at least ~10.0 W peak optical output power (Fig. 3a), and a peak WPE of 47% at 80 K (Fig. 3b). The WPE further increases to >48% at 9 K. If taking into account the 0.35 Ω measured wiring resistance from the power source to the laser, the laser reaches 50% WPE at 9 K. Even at 200 K the peak WPE is still ~35%. Figure 4 shows a scatter plot of the peak WPE at 80 K for all tested lasers with cavity lengths varying from 2.3 to 3.0 mm. The majority of the tested devices in this cavity length range have a peak WPE greater than 40% at 80 K, and several have a peak WPE greater than 45% (this plot has not been corrected for the wiring resistance). These results are a significant improvement compared to the best reported results[10], and surpass the WPE limit generally predicted for conventional QCLs. A low waveguide loss of ~1.5 cm^{-1} is extracted from '$1/L$' measurements, which is also helpful for achieving a high laser WPE. Two advantageous features of this design, that is, the greatly improved maximum current density and the relatively high slope efficiency, are maintained at high temperatures. The slope efficiency drops <5% from 9 to 160 K, and in the temperature range from 160 to 300 K a very high characteristic temperature of the slope efficiency T_1 of ~330 K is extracted, whereas in conventional QCLs the T_1 is usually below 300 K in the same temperature range. A characteristic temperature T_0 of ~125 K is extracted from the threshold current density versus temperature characteristics. This lower than ideal value is largely due to the low two-LO-phonon voltage defect used in the injector for this particular design, which favours low-temperature operation and limits the laser threshold performance and WPE at high temperature.

The lasers have also been characterized in continuous-wave (c.w.) mode operation at cryogenic temperatures. The laser shown in Fig. 3 has a peak c.w. power of at least 6.0 W and 4.5 W at 30 K and 80 K, respectively (Fig. 5a). Maximum values for the c.w. WPE of 32% at 30 K and 28% at 80 K are extracted (Fig. 5b).

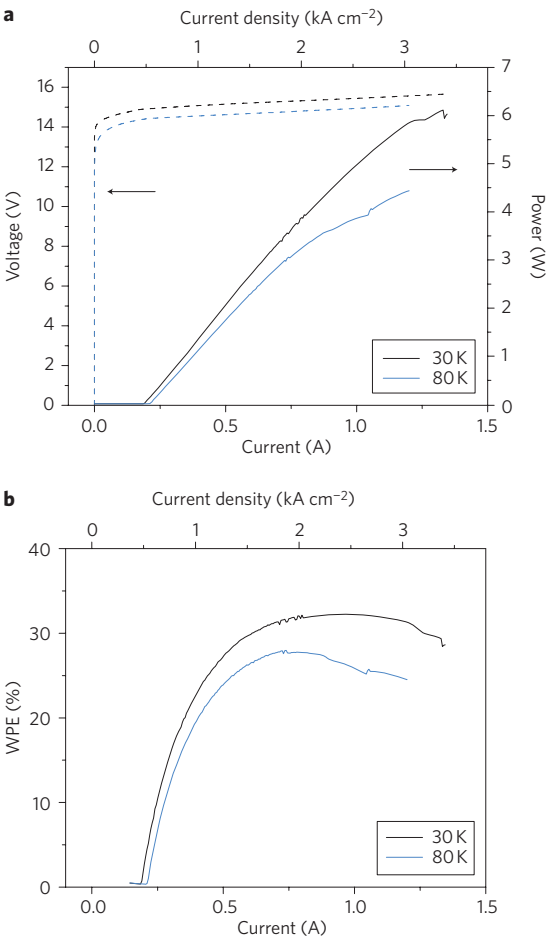

Figure 5 | Continuous-wave light–current–voltage measurements and extracted WPE. a, Continuous-wave light–current–voltage measurement for the same laser as shown in Fig. 3 at heat sink temperatures of 30 and 80 K. The measured single-facet optical power is doubled for two facets and corrected for an optical collection efficiency of 74%. **b**, The plot of c.w. WPE versus current is extracted from the experimental results in **a**.

They are significantly lower, however, than the corresponding pulsed results at the same temperatures. This is largely due to lack of an efficient heat removal mechanism, as these lasers were not fabricated and packaged for c.w. operation. Characterization of the back-facet high-reflectivity-coated buried-heterostructure lasers shows an improved c.w. performance in terms of maximum usable output power, maximum operating temperature and WPE (Supplementary Fig. S3).

In summary, we have experimentally realized a new design of QCL that uses an ultrastrong coupling between the injector and active regions. This new design overcomes the interface-roughness-induced detuning of resonant tunnelling between the injector ground level and the upper laser level, and more effectively facilitates electron transport across the quantum cascade and, in turn, greatly improves QCL performance, such as power, slope efficiency and especially WPE. An unprecedented 50% WPE is experimentally demonstrated.

Received 26 May 2009; accepted 16 November 2009; published online 10 January 2010

References

1. Faist, J. *et al.* Quantum cascade laser. *Science* **264,** 553–556 (1994).
2. Gmachl, C., Capasso, F., Sivco, D. L. & Cho, A. Y. Recent progress in quantum cascade lasers and applications. *Rep. Prog. Phys.* **64,** 1533–1601 (2001).

3. Wang, Q. J. *et al.* High performance quantum cascade lasers based on three-phonon-resonance design. *Appl. Phys. Lett.* **94,** 011103 (2009).
4. Bai, Y., Slivken, S., Darvish, S. & Razeghi, M. Room temperature continuous wave operation of quantum cascade lasers with 12.5% wall plug efficiency. *Appl. Phys. Lett.* **93,** 021103 (2008).
5. Khurgin, J. B. *et al.* Role of interface roughness in the transport and lasing characteristics of quantum-cascade lasers. *Appl. Phys. Lett.* **94,** 091101 (2009).
6. Sirtori, C. *et al.* Resonant tunneling in quantum cascade lasers. *IEEE J. Quantum Electron.* **34,** 1722–1729 (1998).
7. Faist, J. Wallplug efficiency of quantum cascade lasers: critical parameters and fundamental limits. *Appl. Phys. Lett.* **90,** 253512 (2007).
8. Offermans, P. *et al.* Digital alloy interface grading of an InAlAs/InGaAs quantum cascade laser structure studied by cross-sectional scanning tunneling microscopy. *Appl. Phys. Lett.* **83,** 4131–4133 (2003).
9. Faist, J. *et al.* Bound-to-continuum and two-phonon resonance quantum-cascade lasers for high duty cycle, high-temperature operation. *IEEE J. Quantum Electron.* **38,** 533–546 (2002).
10. Gresch, T., Giovannini, M., Hoyer, N. & Faist, J. Quantum cascade lasers with large optical waveguides. *IEEE Photon. Tech. Lett.* **18,** 544–546 (2006).

Acknowledgements

The authors would like to acknowledge the collaboration with J. Meyer and his team at the Naval Research Laboratory, Washington, DC. This work is supported in part by the Mid-InfraRed Technologies for Health and the Environment (MIRTHE) Research Center (National Science Foundation—Engineering Research Centers) and the Defense Advanced Research Projects Agency—Efficient Mid-Wave Infrared Lasers Program.

Author contributions

P.Q.L. carried out the design, fabricated the devices, performed the measurements and analysed the data. A.J.H. and M.D.E. contributed to the measurements and data analyses. K.J.F. developed the design tools. J.B.K. and Y.D. proposed the idea and carried out the theoretical calculations. X.W. conducted the MOCVD growth of the samples. J.-Y.F. contributed to the device fabrication. C.F.G. supervised the whole project and, together with P.Q.L., prepared the manuscript.

Additional information

The authors declare no competing financial interests. Supplementary information accompanies this paper at www.nature.com/naturephotonics. Reprints and permission information is available online at http://npg.nature.com/reprintsandpermissions/. Correspondence and requests for materials should be addressed to P.Q.L.